Phonon Induced Contrast in Matter Wave Interferometer

Qian Xiang,[1] Run Zhou,[1] Sougato Bose,[2] and Anupam Mazumdar[1]

[1]*Van Swinderen Institute, University of Groningen, 9747 AG, The Netherlands*
[2]*Department of Physics and Astronomy, University College London, Gower Street, WC1E 6BT London, UK*

Utilizing the Stern-Gerlach apparatus to create matter-wave superposition states is a long-sought-after goal, not only due to its potential applications in the quantum realm but also because of its fundamental implications for studying the quantum properties of gravity. The main challenge in creating a macroscopic quantum interferometer arises from the loss of coherence, primarily through two channels. One channel involves strong coupling with the environment for macroscopic matter, leading to decoherence. The other channel relates to the precision of wave packet overlap, which can occur due to external and internal fluctuations of various sources. The latter introduces a unique challenge for larger-scale masses by perturbing the centre of mass motion of the macroscopic object. Here, we study a particular challenge, namely, the issue of internal degrees of freedom, specifically phonon fluctuations and contrast reduction. This work will investigate the contrast reduction caused by spin-magnetic field and diamagnetic interactions at the phonon occupation level in the quantum gravity-induced entanglement of masses (QGEM) protocol configuration.

1. INTRODUCTION

The matter-wave interferometer is an essential tool for generating sizeable spatial superposition states. It represents the forefront of theoretical physics, as the creation of spatial superposition states can aid in constructing a theory that reconciles gravity with quantum mechanics[1–5], studying the equivalence principle[6–9], decoherence mechanism[10–22]. In terms of applications, matter-wave interferometers are also considered for detecting gravitational waves[23], neutrinos [24], detecting light axion-like particles [25], for precise measurements of Earth's gravitational acceleration[23, 26–33], and detection of space debris [34].

To test the quantum nature of gravity, a proposal known as quantum gravity induced entanglement of masses (QGEM) has been recently proposed [35] [1]. To further probe the nature of gravity, the gravitational-optomechanical test, which tests the analogue of light-bending experiment in quantum gravity [38], and measurement-based tests [39], all require the creation of a matter-wave interferometer.

The QGEM proposal utilizes the two masses, each prepared in a spatial superposition state, which is kept at a distance where the only interaction between them is mediated via gravity. If detectable entanglement exists between these two masses, one can ascertain that the gravitational interaction is quantum in nature [40–46]. This quantum-entanglement-based, experimental is concordant with the LOCC theorem, which states that classically one cannot mediate quantum entanglement between the two quantum systems [47].

In QGEM, the spatial superposition is created by the Stern-Gerlach (SG) apparatus [48] while the test mass is played by a diamond internally embedded with a nitrogen-vacancy centre (NV). The SG device utilizes the coupling between the magnetic field and the spin (NV-centre) to create a spatial superposition state. Based on similar mechanisms, there have been approaches toward atom interferometry. Such interferometer has been experimentally realized on atom chips for half-loop [49] and full-loop [50] schemes. For the former, the coherent time for maintaining spatial superposition was 21.45 ms, and the size of 3.98 μm was reached. For the full loop, the coherent time and superposition size were 7 ms and 0.38 mum, respectively.

Of course, QGEM imposes higher demands on the interferometer's performance, with critical requirements including the diamond's mass $M \sim 10^{-15} - 10^{-14}$ kg and the spatial superposition size needing to reach approximately $10 - 100\mu$m [15, 18, 22, 35], and [51]. The larger mass objects tend to couple more strongly with their environment, such as the electromagnetic fields and collisions with residual gas particles. These couplings act as measurements, causing the collapse of the spatial superposition state into classical states, known as decoherence [52, 53]. Furthermore, due to experimental constraints on the magnetic field gradient [54, 55], the time required to achieve large-scale spatial superposition states is on the order of $\Delta t \sim 1$ second makes it more challenging to maintain the spin coherence state of NV centres and the spatial superposition state of diamond [2].

For a closed-loop scheme, another challenge that is independent of the environment arises from the Humpty-Dumpty (HD) effect[58–61], which refers to the overlap problem of matter waves. For example, in the atomic interferometer mentioned above, if the wave packets on both sides of the interferometer arm cannot precisely overlap (both in translational and rotational degrees of

---

freedom), they cannot generate interference fringes and thus lead to the loss of contrast, see [62] where the analysis of HD effect has been analysed quite nicely including the impact of angular momentum and the libration mode of the NV spin. For macroscopic objects, there is also a challenge of overlap due to the internal degrees of freedom, such as phonon vibration. In a very interesting work[63], the contrast reduction of phonon wave packets induced by coupling NV centres with magnetic fields was demonstrated. More recently, this coupling has been extended to white noise, providing a boundary on creating larger-scale spatial superposition states that have been considered [64].

This work will also investigate the contrast loss caused by phonons in matter-wave interferometers. Unlike atomic-scale interferometers, due to the diamagnetic property of a diamond and its interaction with the magnetic field being proportional to its mass, the diamagnetic interaction becomes essential in the matter-wave interferometers with a massive object. For example, the diamagnetic interaction contributes to the trajectories of the diamond's centre of mass (CoM) wave packets. Therefore, the magnetic field must be carefully designed to guarantee a close loop[54, 65–67]. Besides, there has been recently proposed a mass-independent scheme[67] based on diamagnetic interaction of creating large superposition size. From the perspective of internal degrees of freedom, the diamagnetic repulsions of the diamonds on either side of the interferometer arms are different, leading to the excitation of varying phonon modes and thus resulting in a contrast reduction of internal degrees of freedom. This is fundamentally similar to the spin-magnetic field interaction papers [63, 64].

In this regard, our paper differs from the Refs.[63, 64]. We validate their results for the spin-magnetic field interaction. However, we also Consider the effect of diamagnetic contribution, which brings another layer of complexity that is not present otherwise. In the case of diamagnetic contribution, the phonons are also coupled to the CoM of the diamond, intrinsically bringing a new kind of interaction. The difference lies in the fact that for diamagnetic interaction, each carbon atom in the atomic chain on both sides of the interferometer arms experiences repulsion in the same direction, while for the spin-magnetic interaction, the chains are plucked at the NV-centre in opposite directions, as illustrated in Fig. 1. Besides the magnetic effects, we will also briefly mention the role of electric dipole interaction with phonons and how it affects the latter in comparing the loss of contrast for the one-loop interferometer.

The structure of this work is arranged as follows. In section 2, we introduced the setup, which includes the phonon model and the statistical model of phonon modes at finite temperature, and introduced the Wigner function. In 3, we provided the Hamiltonian of the diamond and presented the model for the trajectory of the diamond wavepacket. In 4, we examined the different effects of diamagnetic repulsion and spin-magnetic field interac-

tion on phonon dynamics and further utilized displacement operators in Section 5 to describe the phonon's contrast reduction. In Section 6, we presented numerical results and compared the contrast loss induced by these two interactions at different temperatures. Also, we have considered contrast loss led by other interactions, potential dipole-electric field interaction, in the level of phonon; this part of the discussion can be found in Appendix C and D.

2. BRIEF REVIEW ON PHONON

Phonons constitute the primary focus of this work, and the model is derived from the lattice chain model, see Ref.[68]. In the case of atomic interactions, the Hamiltonian for free phonons can be expressed as follows,

$$
\begin{aligned}
H_{\text{free}} &= m \sum_i \frac{\dot{x}_i^2}{2} + \sum_{i,j} \frac{K_{ij}}{2} x_i x_j \\
&= \sum_q \frac{1}{2} \left(\dot{u}_q^2 + \omega_q^2 u_q^2 \right),
\end{aligned}
\tag{1}
$$

where K_{ij} is a matrix associated with the inter-atomic interaction while $Q_q(X_i) = Q_q^i$ represents the eigenvector of the matrix. The position of each atom can be represented as $X_i(t) + x_i(t)$, where the capital $X_i(t)$ denotes the equilibrium position of the ith atom at any instant of time, and x_i represents its small vibrations. Because the position of the diamond as a whole varies within the SG apparatus, the equilibrium position $X_i(t)$ of each atom in the chain becomes a function of time. Notably, the relative distances between these equilibrium positions, $X_{i+1} - X_i = \text{const.}$, remain constant. Therefore, $X_i(t)$ can effectively be regarded as the trajectory of the diamond, with their distances relative to the centroid $X_{\text{c(enter)}}$ remaining unchanged. Here, for convenience, we assume that the NV centre within the atom is embedded at the centroid's position, $X_{\text{s(pin)}}(t) = X_{\text{c}}(t)$. In the following, we sometimes neglect the time t for convenience.

The small movement $x_i(t)$ can be expanded into mode amplitude u_q, with creation and annihilation operators as,

$$
x_i(t) = \frac{1}{\sqrt{Nm}} \sum_q Q_q^i u_q(t),
\tag{2}
$$

where the relation between u_q and its conjugate (the momentum $\dot{u}_q$), and the creation and annihilation operator can be expressed as,

$$
\begin{aligned}
a_q &= \frac{1}{\sqrt{2\hbar\omega_q}} (\omega_q u_q + \mathrm{i}\dot{u}_q), \\
a_{-q}^\dagger &= \frac{1}{\sqrt{2\hbar\omega_q}} (\omega_q u_q - \mathrm{i}\dot{u}_q).
\end{aligned}
\tag{3}
$$

For simplicity, in our one-dimensional atomic chain model embedded with an NV centre, we assume that
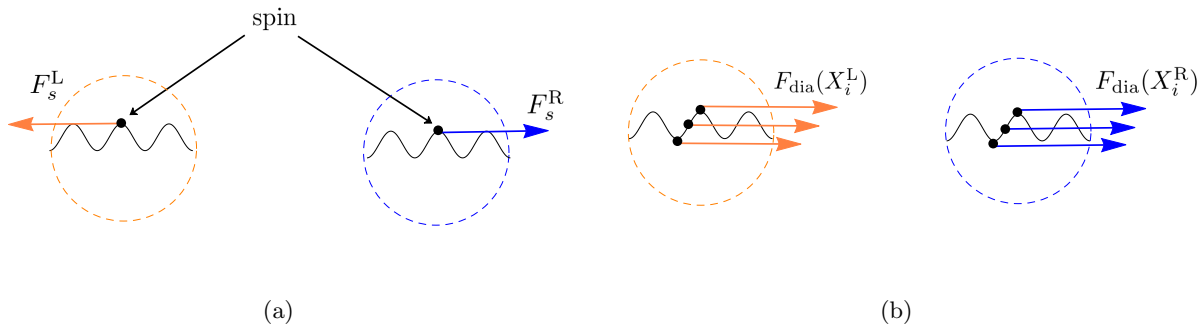
FIG. 1: Illustrations of different forces acting on a lattice chain (represented by black solid wave lines) where positions of atom/spin are dotted in black. The wave packets of the centre of mass (CoMs) in the two interferometry arms denoted here by the left (L) and right (R) arms are plotted by orange and blue circles. Panel (a) shows splitting forces $F_s^{\mathrm{L,R}}$ acting on the spin with site number s have the same magnitude but opposite direction. Panel (b) shows diamagnetic forces $F_i^{\mathrm{L,R}}$ acting on every atom, where, for simplicity, we assume it acts on the spin as well without changing the main dynamics of the chain.

all particles have identical mass, and the total mass is given by $M = Nm$, where N is the total number of particles in the diamond, and m is the atomic mass of the diamond. The ω_q is the eigen-frequency of the chain model with fundamental tone $\omega_0 = \pi c/L$, where $c = 17.5 \times 10^3 \mathrm{m/s}$ is the sound speed within a diamond [68] and L is the length. For example, for the masses in a range $M \sim 10^{-14} \sim 10^{-20}$ kg the corresponding fundamental tone ranges from $\omega_0 \sim 10^{10} - 10^{12}$ Hz.

At the initial stage, $t = 0$, before the diamond enters the SG apparatus and interacts with the magnetic field, one can assume that the phonons are in a thermal equilibrium state at a temperature T [68],

$$\langle n_q(t = 0) \rangle = \frac{1}{2} \coth\left(\frac{1}{2}\frac{\hbar\omega_q}{k_{\mathrm{B}}T}\right). \quad (4)$$

According to the equipartition theorem, one can establish the relationship between the average number of phonons $\langle n_q(0) \rangle$, the characteristic length σ_{u_q} and the characteristic momentum $\sigma_{\dot{u}_q}$ as [68],

$$\langle n_q(t = 0) \rangle = \frac{\omega_q}{\hbar}\sigma_{u_q}^2 = \frac{1}{\hbar\omega_q}\sigma_{\dot{u}_q}^2, \quad (5)$$

where σ_{u_q} and $\sigma_{\dot{u}_q}$ are statistical averages. A review of this detail can be found in the appendix A. In the case of thermal equilibrium, the phonons in each mode q form a mixed state. The amplitudes and momenta of the phonons thus take on Gaussian distributions, represented by the Wigner function[69] as follows,

$$W(u_q, \dot{u}_q) = \mathcal{N} \exp\left[-\left(\frac{u_q^2}{2\sigma_{u_q}^2} + \frac{\dot{u}_q^2}{2\sigma_{\dot{u}_q}^2}\right)\right], \quad (6)$$

where $\mathcal{N}$ is normalization factor. Eq. (5) gives the normal mode's characteristic length and momentum. Note that σ_{u_q} and $\sigma_{\dot{u}_q}$ are statistical averages dependent on temperature T, see appendix A. Once we let the diamond experience the SG force, the occupation number of the phonons will evolve, and we will estimate that in the following sections.

3. INTERACTIONS IN STERN-GERLACH APPARATUS

For the diamond embedded with a single spin S in the NV, we already assume that it has been prepared in a superposition of opposite direction $S^{\mathrm{R}} = 1$ (right) and $S^{\mathrm{L}} = -1$ (left), hence the spatial superposition. The Hamiltonian for the diamond's CoM consists of three parts [3],

$$H_{\mathrm{CoM}} = \frac{P_c^2}{2M} - \mu S^{\mathrm{L,R}}B - \frac{\chi_\rho M}{2\mu_0}B^2, \quad (7)$$

the first term is just the kinetic energy relating to CoMs's momentum. The second term is the spin-magnetic field coupling with the magnetic moment $\mu = g\mu_{\mathrm{b}}$, where the Landé g-factor $g \approx 2$ and Bohr magneton $\mu_{\mathrm{b}} = 9.27 \times 10^{-24}$ (J/T). For simplicity, we assume the NV-centre is located at the centre of mass of the diamond with equilibrium position $X_s = X_c$. The third term relates to diamagnetic energy with mass susceptibility $\chi_\rho = -6.2 \times 10^{-9}\mathrm{m^3/kg}$ and vacuum permeability μ_0.

For the magnetic field in Eq. (7), we give its form that is experienced by the ith atom as,

$$B_i(t) = B_0 + b(t)X_i(t), \quad (8)$$

where B_0 is the bias magnetic field, and $b(t)X_i(t)$ denotes the gradient in the SG setup experienced by the ith atom. Note that in Eq.(8), the coordinates along the $\mathbf{e}_x$-axis are represented by the uppercase X_i, indicating the equilibrium positions of atoms in the chain. For example, the magnetic field experienced by the spin, which

---

[3] There is also a term related to $D(S\cdot\hat{n})^2$ related to the zero-point splitting [62, 65]. This term is relevant for the internal spin degrees of freedom. Here, we are not considering this contribution; we do not consider the rotation of the diamond in our current context.

we have assumed to be located at the centre of the chain, becomes $B_c = B_0 + b(t)X_c$. In this model, we only consider the one-dimensional case, where the separation of the diamond and the force on the atomic chain is confined to the $\mathbf{e}_x$ direction.

We do not consider the motion of the diamond in other dimensions, such as in drop tower experiments where the diamond needs to move in the direction of Earth's acceleration or in magnetic levitation setups where it moves along a direction orthogonal to $\mathbf{e}_x$. In these cases, the form of a magnetic field becomes very complicated for a closed loop, and it needs a careful design, especially when one takes the diamagnetic term into account [67, 70]. For simplicity, we consider the movements of CoMs only along $\mathbf{e}_x$, and they are subjected only to the spin-magnetism interaction (second term in Eq. (7)). Therefore, to get a closed loop, the magnetic gradient $b(t)$ can be expressed in a very simple form as [56],

$$
b(t) = \begin{cases} +\eta_{\mathrm{b}}, & t = [t_1, t_2] \\[4pt] -\eta_{\mathrm{b}}, & t = [t_2, t_3] \\[4pt] 0, & t = [t_3, t_4] \\[4pt] -\eta_{\mathrm{b}}, & t = [t_4, t_5] \\[4pt] +\eta_{\mathrm{b}}, & t = [t_5, t_6] \end{cases} \tag{9}
$$

where in different time intervals, the gradients take constant values $\pm\eta_{\mathrm{b}}$. The closed loop is guaranteed as long as the acceleration and deceleration durations are the same. So far, we can observe from the Hamiltonian Eq. (7) that the diamond experiences two types of forces, i.e., the separation force acting on the NV-centre particle located at the centre X_c, and the diamagnetic force exerted by the entire diamond. Regarding the former, the force acts only on the central particle, the spin, which can be read out by doing partial derivative to the second term in Eq. (7), which has the form,

$$
F_{\mathrm{s}}^{\mathrm{L,R}}(t) = \mu S^{\mathrm{L,R}} b(t), \tag{10}
$$

where subscript represents the spin. From here, one can immediately write down the interaction between the magnetic field and phonon as $-F_{\mathrm{s}} x_c$, which we will discuss in the following section. The tiny vibration of the NV-centre is imparted by $x_c(t)$, and the characteristic of the unique centre position is captured by the eigen-vector $Q_q^c(t)$ introduced in Eq. (2). Here, we keep labelling the spin-magnetic force as $F_{\mathrm{s}}^{\mathrm{L,R}}$ to distinguish it from the following diamagnetic force. But one should note that $F_{\mathrm{s}}^{\mathrm{L, R}}$ acts on the CoM, $X_c(t)$, and it is responsible for the trajectories of the diamond.

The diamagnetic force acts on the entire diamond effectively at the positions of CoMs $X_c^{\mathrm{L, R}}$. Here, we make an assumption that the diamagnetic force experienced by the entire diamond can be equally distributed to each individual atom inside the diamond.

$$
F_{i,\mathrm{dia}}^{\mathrm{L,R}}(t) = F_c^{\mathrm{L,R}}(t) = \frac{\chi_\rho M}{N\mu_0}\left(B_0 b + b^2 X_c^{\mathrm{L,R}}(t)\right). \tag{11}
$$

Note that the diamagnetic force acting on each atom (including the NV centre for convenience) is equal to the diamagnetic force experienced by the CoMs of wave packets of diamond divided by the total number of atoms N. Here, $F_c^{\mathrm{L,R}}$ represents the diamagnetic force experienced by any arbitrary atom i^{th} inside the diamond. And the phonon-diamagnetic force coupling can now be written as $-F_{i,\mathrm{dia}}^{\mathrm{L,R}} x_i = -F_c^{\mathrm{L,R}} x_i$ (summed over i and mode q).

Recalling that we use a linear magnetic field, this simple magnetic field is widely applied in interferometers [54, 71]. Since the magnetic field gradient can be modelled as a step function, the separation force Eq. (10) acting on the spin is independent of its equilibrium position $X_{s(c)}$. Therefore, there is no coupling between the trajectories of wave packets and the phonon degrees of freedom.

In contrast to the splitting force acting on the NV centre, the situation for the diamagnetic force (11) acting on each particle in the atomic chain is more complicated. The tiny vibrations of these particles (phonons) are coupled to their equilibrium positions (trajectories) through the magnetic field (considering $F_c^{\mathrm{L,R}} \times x_i$ for each particle). Additionally, as shown in Fig. 1 (a), the forces acting on the NV centre in different wave packets are of the same magnitude but in opposite directions. Therefore, when the loop is completed, the contrast of phonons modes always differs by a positive or negative sign in both normal coordinates and momentum. For the diamagnetic force in Fig. 1 (b), the corresponding atoms in the atomic chain of the two wave packets experience the same direction of diamagnetic force but with different magnitudes (depending on the scale of spatial superposition). It is not difficult to imagine that the phonon modes will exhibit contrast reduction under such differential influences.

In this toy model, we only investigate the contrast loss of phonon modes; the mismatch issue with the external degrees of freedom is beyond the scope of this work. We assume perfect overlap of the equilibrium positions (CoMs as well as $X_i^{\mathrm{L,R}}$), a necessary assumption also employed in the seminal works [63, 64]. Thus, we consider a simplified trajectory scenario where the trajectory of the diamond wave packets is solely governed by the spin-magnetic field coupling (10). In this simplest case, the equilibrium positions of corresponding particles in the two wave packets are symmetric given by $X^{\mathrm{R}} = -X^{\mathrm{L}}$, as illustrated in Fig. 2. The maximum accelerations of the two paths are thus a series of constants given by,

$$
a^{\mathrm{L,R}}(t) = \frac{\mu S^{\mathrm{L,R}} b(t)}{M}, \tag{12}
$$

we assume that at the initial moment, the spin inside the diamond has been prepared in a superposition, and the
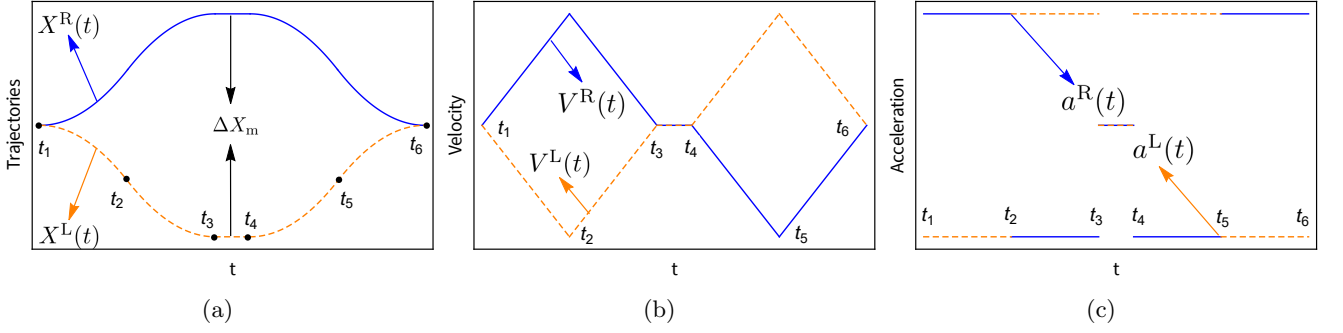
FIG. 2: Illustrations of matter wave packet trajectories shown in panel (a), velocities in panel (b) and acceleration protocols in panel (c), where blue lines represent CoM wave packet on the right ($S = S^{\mathrm{R}}$) and orange dash lines represent the left ($S = S^{\mathrm{L}}$). Duration of acceleration and deceleration in time intervals $[t_1,\ t_2]$, $[t_2,\ t_3]$, $[t_4,\ t_5]$, $[t_5,\ t_6]$ are the same and is denoted as a positive value τ_a. During the time interval $[t_3,\ t_4]$, we assume a free-flight process of wave packets with zero acceleration. The duration of this process is denoted as $2\tau_{\mathrm{f}}$. The total duration for wave packets flying in the SG apparatus is therefore $4\tau_{\mathrm{a}} + 2\tau_{\mathrm{f}}$.

CoM of the diamond is at rest. When the loop starts, the magnetic field gradient $b(t)$ takes the protocol as mentioned in Eq.(9). In this toy model, we are neglecting the acceleration due to the induced diamagnetic potential for the time being. In fact, including the effect will not modify the current scenario a lot, as what matters is the relative force difference between the left and the right trajectories of the interferometer.

As depicted in Fig. 2 (c), under the given magnetic field gradient settings, the acceleration of the CoMs also exhibits a series of step functions. The blue and orange line segments correspond to the trajectories of S^{R} and S^{L}, respectively. The corresponding trajectories are shown in Fig. 2 (a), and they can be expressed by the following expressions,

$$
X_c^{\mathrm{L,R}}(t) = \begin{cases} \frac{a^{\mathrm{L,R}}(t+2\tau_{\mathrm{a}}+\tau_{\mathrm{f}})^2}{2}, & t = [t_1, t_2] \\[2mm] \frac{a^{\mathrm{L,R}}\left(t^2-2\tau_{\mathrm{a}}^2+2\tau_{\mathrm{f}}t+\tau_{\mathrm{f}}^2\right)}{2}, & t = [t_2, t_3] \\[2mm] a^{\mathrm{L,R}}\tau_{\mathrm{a}}^2, & t = [t_3, t_4] \\[2mm] \frac{a^{\mathrm{L,R}}\left(t^2-2\tau_{\mathrm{a}}^2-2\tau_{\mathrm{f}}t+\tau_{\mathrm{f}}^2\right)}{2}, & t = [t_4, t_5] \\[2mm] \frac{a^{\mathrm{L,R}}(-t+2\tau_{\mathrm{a}}+\tau_{\mathrm{f}})^2}{2}, & t = [t_5, t_6] \end{cases} \tag{13}
$$

Thus, the relative separation distance $\Delta X(t)$ between the two trajectories is also a quadratic function of time. During the time interval $[t_3, t_4]$, this distance between the two trajectories reaches its maximum value,

$$
\Delta X_{\mathrm{m}} = 2\left|a^{\mathrm{L,R}}\right|\tau_{\mathrm{a}}^2, \tag{14}
$$

where we defined the positive constant maximum acceleration $\left|a^{\mathrm{L,R}}\right| = \mu\eta_{\mathrm{b}}/M$, and total duration time $\Delta t = t_6 - t_1$.

4. PHONON FLUCTUATIONS

In this section, we will investigate the impact of the above-mentioned interaction forces, see Eqs. (10, 11), acting on the lattice chain on the contrast of phonon wave packets. Here, we generally represent the aforementioned forces as $F_i(X_i^{\mathrm{L,R}})$ (we will neglect $X_i^{\mathrm{L,R}}$ for simplicity sometimes and use just $F_i^{\mathrm{L,R}}$). The total Hamiltonian regarding every atom and their interactions with external fields can be written as,

$$
\begin{aligned} H_{\mathrm{tot}} &= H_{\mathrm{free}} - \sum_i F_i^{\mathrm{L,R}} x_i \\ &= H_{\mathrm{free}} - \sum_{i,q} \frac{Q_q^i F_i^{\mathrm{L,R}}}{\sqrt{M}} u_q, \end{aligned} \tag{15}
$$

where H_{free} is the free phonon Hamiltonian mentioned in Eq. (1). Eq. (15) represents the energy change of the diamond interacting with the magnetic field after entering the SG apparatus.

When the diamond enters the SG apparatus, the interaction between its internal particles and the external field changes the number of phonons. With the Hamiltonian Eq. (15), the kinematic equations for the canonical coordinates of each vibrational mode q can be derived as,

$$
\ddot{u}_q + \omega_q^2 u_q := f_q^{\mathrm{L,R}} = \sum_i \frac{Q_q^i F_i^{\mathrm{L,R}}}{\sqrt{M}}, \tag{16}
$$

where f_q encompasses the forces acting on all atoms, it can be regarded as the force acting on the lattice chain. The solution of Eq. (16) is,

$$
\begin{aligned} u_q(t) =& u_q(0)\cos(\omega_q t) + \dot{u}_q(0)\frac{\sin(\omega_q t)}{\omega_q} \\ &+ \int_0^t \frac{\sin\omega_q(t-t')}{\omega_q} f_q^{\mathrm{L,R}}(t')\,\mathrm{d}t'. \end{aligned} \tag{17}
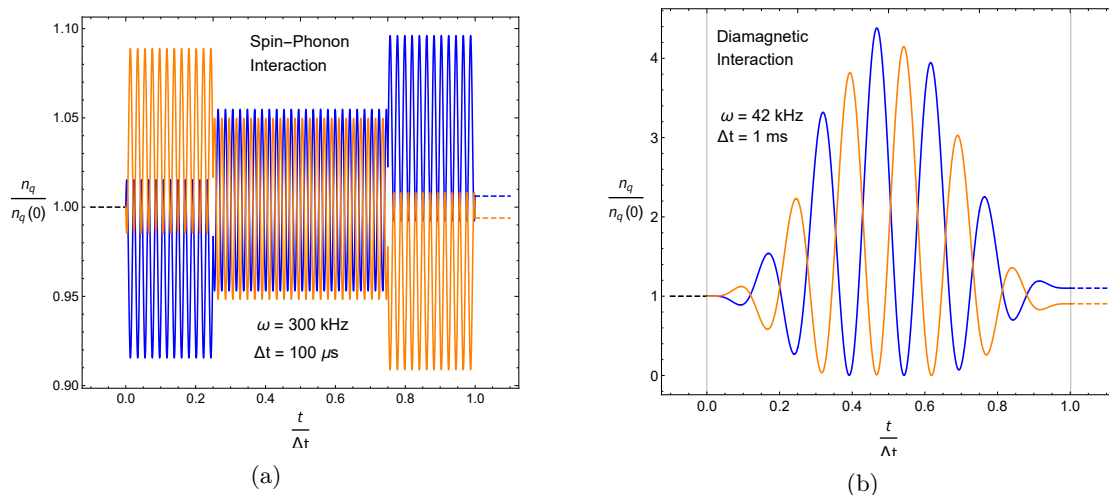$$

FIG. 3: The occupation numbers of the phonons for the spin-magnetic field interaction shown in panel (a), and for the the diamagnetic force shown in panel (b). The blue and orange curves represent the wave packets of the diamond on the right and left sides, respectively. The black dashed line represents the number of phonons in the diamond before entering the SG device (scaled to one), and the blue and orange dashed lines represent the number of phonons on both sides after the closure of the trajectory of the diamond's CoMs.

Here, the initial conditions, the phonon amplitude $u_q(t = 0)$, and its conjugate momentum $\dot{u}_q(t = 0)$ are solely dependent on the initial temperature of the diamond Eq. (5). The initial phonon population in mode q is (4) for the thermal equilibrium mixed state considered here. From here, it can be observed that due to the difference in forces acting on the atomic chains on the two sides of the interference arm, a discrepancy exists in the population of phonons with mode q.

$$n_q(t) = \frac{1}{2\hbar\omega_q}\left(\dot{u}_q^2 + \omega_q^2 u_q^2\right). \tag{18}$$

Recall that $F_i^{\mathrm{L,R}}$ in (16) is a generalized form introduced for convenience. When investigating spin-magnetic field coupling, it needs to be substituted with (10). In this case, the summation over atomic index i disappears (we consider only a single NV-centre). When studying the influence of the diamagnetic force of the lattice chain in different trajectories on internal degrees of freedom, $F_i^{\mathrm{L,R}}$ is replaced by (11), and the summation in (16) should include all atoms.

In Fig. 3, we have separately illustrated the differences in the number of phonons induced by these two types of forces (10, 11). Recall that the eigenvector Q_i^q of phonons is a quantity related to the atom index i^{th}. Here, we choose it to be one as the upper limit. the number of phonons is constant at the initial moment. After the diamond enters the SG apparatus, the number of phonons in the two trajectories changes differently and stabilizes with a constant difference after the duration time Δt. Recall that we are interested in diamond masses ranging from $M \sim 10^{-20}$ to 10^{-14} kg with frequencies ω_q in the range of $\omega_q \sim 10^{10} - 10^{12}$ Hz. Therefore, the rate of change of the population of phonons of mode q

is extremely rapid. Here, for visual clarity, we plot the variation in the number of low-frequency phonons in two types of interactions. One should note that due to the size constraints of diamonds ($\omega_0 = \pi c/L$), elastic waves in the material do not reach such low frequencies. The change of phonon number is small in the high-frequency range and becomes a perturbation.

Here, we introduce the difference in phonon amplitude and momentum on both sides of the interferometer arms, which arise from $f_q^{\mathrm{L,R}}$.

$$\begin{aligned}\Delta u_q &= \int_0^t \Delta f_q(t')\frac{\sin\omega_q(t-t')}{\omega_q}\,\mathrm{d}t' \\ \Delta\dot{u}_q &= \int_0^t \Delta f_q(t')\cos\omega_q(t-t')\mathrm{d}t',\end{aligned} \tag{19}$$

where we define $\Delta f_q = f_q^{\mathrm{R}} - f_q^{\mathrm{L}}$. From here, one can observe that due to the spatial superposition of CoM's, the lattice chain in the two wave packets experiences different forces. In Fig. 4, we illustrate the differences in the phase space of phonon wave packets from different paths. For visual clarity, the early stage of phase evolution is faded out, and normal coordinate and its conjugate have been made dimensionless. In [63, 64], the authors have shown that the phase space trajectories of phonons exhibit differences because the spin in the lattice is moving toward different directions, as shown in Fig. 4 (a). In the case of diamagnetic interactions, the differences in the force value exerted on the lattice still contribute to the reduction in contrast for phonon wave packets. In the next section, we will estimate the loss of contrast due to phonon fluctuations.

5. LOSS OF CONTRAST

The contrast in the internal degrees of freedom is defined as the inner product of the quantum states of phonons after evolving in the two interferometry arms; for a specific mode q, it becomes,

$$C_q = |\langle \psi_q^{\text{L}}(\Delta t)|\psi_q^{\text{R}}(\Delta t)\rangle|. \qquad (20)$$

From Eq. (20), it can be seen that the contrast is essentially the inner product of normalized phonon wave functions. Thus, a perfect closure of position, momentum, and other relevant degrees of freedom, including phonon vibrations, would yield $C_q = 1$, while an imperfect closure results in $C_q \leq 1$. Contrast loss is defined as the logarithmic part of Eq. (20). We employ the time-dependent perturbation theory in quantum mechanics for the time evolution of phonon quantum states. In Eq. (15), the interaction between phonons and external field in the equation is considered as a small perturbation. Now, we ignore the summation over q and focus on one mode; the Hamiltonian becomes,

$$\begin{aligned} H_q &= \hbar\omega_q a_q^\dagger a_q - \sum_i F_i^{\text{L,R}} x_i \\ &= \hbar\omega_q a_q^\dagger a_q - \sum_i F_i^{\text{L,R}} Q_q^i \sqrt{\frac{\hbar}{2M\omega_q}}(a_{-q}^\dagger + a_q). \end{aligned} \qquad (21)$$

Here, recall that the force $F_i^{\text{L,R}}$ is time dependent and it is subjected to the equilibrium positions $X_i^{\text{L,R}}(t)$ of the atomic chain. Considering that the diamond is in a spatial superposition state, the forces acting on the atomic chains in the two trajectories are different. In the interaction picture, denote the time-dependent perturbation part in Eq. (21) as $V_q(t)$, the quantum state of phonon obeys the Schrödinger equation. The overlap of phonon wavepackets in the two arms becomes,

$$\begin{aligned} &\langle\psi_q^{\text{L}}(\Delta t)|\psi_q^{\text{R}}(\Delta t)\rangle \\ &= \langle\psi_q(0)|\exp\left\{\frac{\text{i}}{\hbar}\int_0^{\Delta t}\text{d}t'\left[V_q^{\text{L}}(t') - V_q^{\text{R}}(t')\right]\right\}|\psi_q(0)\rangle \\ &= \langle\psi_q(0)|U_q^{\text{L},\dagger}U_q^{\text{R}}|\psi_q(0)\rangle, \end{aligned} \qquad (22)$$

where U_q is the time evolution operator,

$$U_q^{\text{L},\dagger}U_q^{\text{R}} = \exp\frac{\text{i}}{\hbar}\left[\Delta\dot{u}_q\hat{u}_q + \Delta u_q\hat{\dot{u}}_q\right], \qquad (23)$$

when computing the second line of Eq.(22), $\Delta\dot{u}_q(t)$ and $\Delta u_q(t)$ emerge, which are precisely defined in Eq.(19). In Eq. (23), one can first consider the case of spin-magnetic field coupling (10). In this case, V_q^{L} and V_q^{R} differ exactly by a positive or negative sign, which is because the forces exerted on the phonon wavepackets on both sides of the interferometer arms happen to be in opposite directions. In this scenario, the amplitudes and momentum of the phonons on both sides of the interferometer arms are

displaced in opposite directions by $\frac{1}{2}\Delta u_q$ and $\frac{1}{2}\Delta\dot{u}_q$, respectively. The contrast of phonon can be comprehended as the probability of its amplitude and momentum staying in the initial state $\psi_q(0)$ [63] as shown in Fig. 4 (a), once these two wave packets are separated, the overlap would not be perfect.

For the diamagnetic interaction, the decrease in contrast is also not difficult to imagine. In this case, the amplitudes and corresponding momentum of the phonons on both sides of the interferometer arms are displaced to varying degrees in the same direction. One can always utilize Eq.(22) to calculate the contrast of the phonon wave function. (details are given in the appendix) as,

$$\begin{aligned} C &= |\langle\psi^{\text{L}}(\Delta t)|\psi^{\text{R}}(\Delta t)\rangle| \\ &= \prod_q\left|\text{Tr}\left[U_q^{\text{L},\dagger}U_q^{\text{R}}|\psi_q(0)\rangle\langle\psi_q(0)|\right]\right| \\ &= \prod_q\left|\text{Tr}\left[U_q^{\text{L},\dagger}U_q^{\text{R}}\rho_q(0)\right]\right|. \end{aligned} \qquad (24)$$

Here, we have considered an initial thermal equilibrium ensemble of phonons composed of a state $\rho_q(0)$.

Note that to evaluate the contrast Eq. (24), it is equivalent to evaluate the mean value of $U_q^{\text{L},\dagger}U_q^{\text{R}}$ which consists of both phonon's "position" and its conjugate. Therefore, it is convenient to calculate the mean value by using the Wigner function, which is a quasi-distribution of phonon's position and momentum in phase space, where for a harmonic mode considered here, it has a form of double Gaussian Eq. (6).

Therefore, in the end, by multiplying the exponential operator with Eq. (6) and integrating over u_q and $\dot{u}_q$, the contrast becomes,

$$\begin{aligned} C_q &= \text{Tr}\left[U_q^{\text{L},\dagger}U_q^{\text{R}}\rho_q(0)\right] \\ &= \exp\left[-\frac{\coth\frac{1}{2}\frac{\hbar\omega_q}{k_BT}}{4\hbar\omega_q}\left|\int_0^{\Delta t}\Delta f_q(t)\text{e}^{\text{i}\omega_q t}\,\text{d}t\right|^2\right] \\ &= \exp\left[-\frac{\coth\frac{1}{2}\frac{\hbar\omega_q}{k_BT}}{4\hbar\omega_q}\left|\Delta\tilde{f}_q(\omega_q)\right|^2\right]. \end{aligned} \qquad (25)$$

The final result of the contrast is an exponential function and is temperature-dependent. Naturally, when $\Delta\tilde{f}_q(\omega_q)$ is zero, interference arms on both sides will exhibit no distinction, and Eq. (25) will yield a result of one. However, if there is a difference in the forces acting on the lattice chain on both sides of the interference arms, then $C \neq 1$, and the loss of contrast [4] is expressed as $\log C$.

---

[4] From the expression of contrast, one can directly see why high temperature will destroy contrast. Suppose $T \to \infty$ for a fixed ω_q then the expression for the exponential part of Eq.(25) goes as, $-\frac{k_BT}{2\hbar^2\omega_q^2}|\Delta\tilde{f}_q|^2 \to -\infty$, therefore $C \to 0$. The transfer function $\Delta\tilde{f}_q$ is always non-zero in our case. In the other limit, when
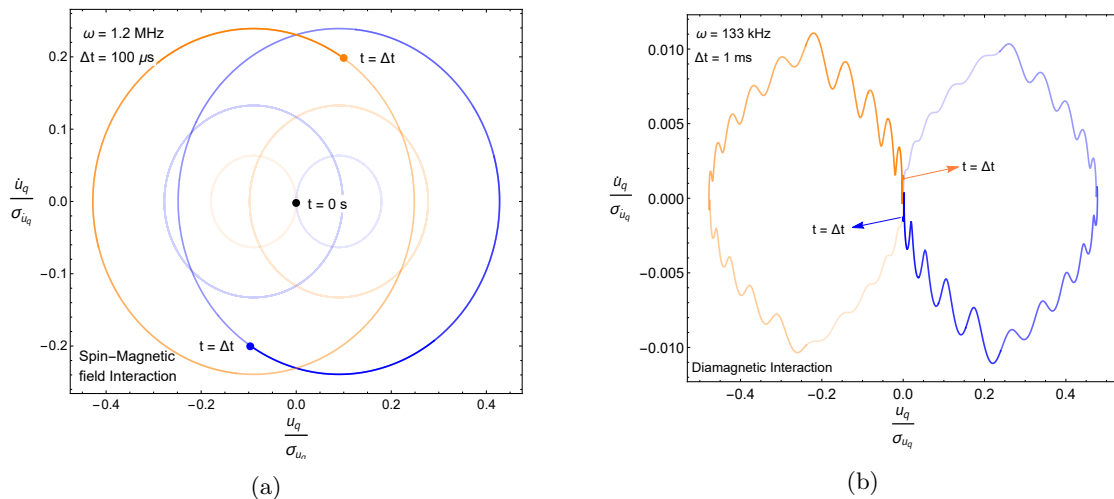
FIG. 4: Illustrations of phonon amplitude in x-axis and momentum in y-axis in phase space. Panel (a) represents the difference induced by spin-magnetic field interaction, and panel (b) shows the phase space due to phonon-diamagnetic force interaction. The blue and orange curves, respectively, represent the wave packets of the diamond on the right and left sides. The early stages of the phase space trajectories are faded for clarity.

The Fourier transform,

$$\Delta \tilde{f}_q := \Delta \tilde{f}_q(\omega_q) = \left| \int_0^{\Delta t} \Delta f_q(t) e^{i\omega_q t} \, dt \right|, \qquad (26)$$

represents a power spectrum that is a function of ω_q and Δt, determining the value and properties of the contrast. In the study of noise in SG devices, macroscopic noise is transformed into the phase fluctuation through this transform. Thus it is also referred to as the transfer function [34] (see also [56]). The transfer function is closely related to the trajectory of the interference arms. For the simplest acceleration protocol (Fig. 1), the transfer function of the splitting force is very trivial, transforming two constant accelerations. The resulting $f_q(\omega_q)$ for this transformation only contains $1/\omega_q$. However, for forces closely related to the trajectory, their transfer function contains powers of $(1/\omega_q)^n$. In the following sections, we will compute the contrast.

6. NUMERICAL RESULTS

In this section, we numerically explore contrast reduction due to phonon wave packets from the interactions given in Eq. (7). Since we do not want the magnetic field gradient, which controls the spatial superposition

---

$\omega_q \sim cq \to 0$, for a finite temperature, again means that the $C \to 0$. Lower values of ω_q can occur for systems with a lower speed of sound. Typically, these are more compressible objects for which the speed of sound is smaller than that of the diamond-like system.
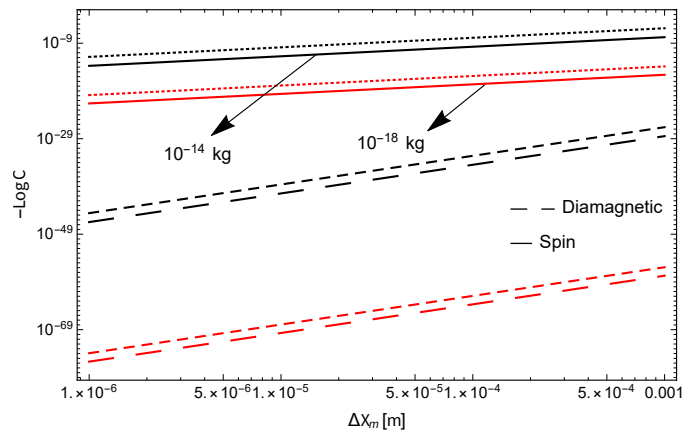

FIG. 5: We show the contrast reduction. Black and red lines correspond to spin-phonon and diamagnetic force-phonon interaction, respectively. Solid and long dash lines represent spin-magnetism and diamagnetic interaction in low temperature (4 K). Dot lines and short dash lines correspond to spin-magnetism and diamagnetic interaction in room temperature (300 K).

state, to be too large ($\eta_b \leq 10^6$) T/m, see such gradients can be achieved in [49, 72], thus the magnetic field gradient determines the maximum spatial separation distances $\Delta X_m \sim 10^{-6} - 10^{-3}$ m for different masses. For simplicity, here we consider phonons as longitudinal elastic waves, $\omega_q = cq$ [68], and treat them as continuous with a minimum frequency (fundamental frequency) $\omega_0 = \pi c/L$. Besides, we take the eigenvector $Q_q^i = 1$ (recall that in solid state physics, these vectors are sinusoidal functions) as an upper limit. We also define the moment when the diamond wavepacket reaches its max-
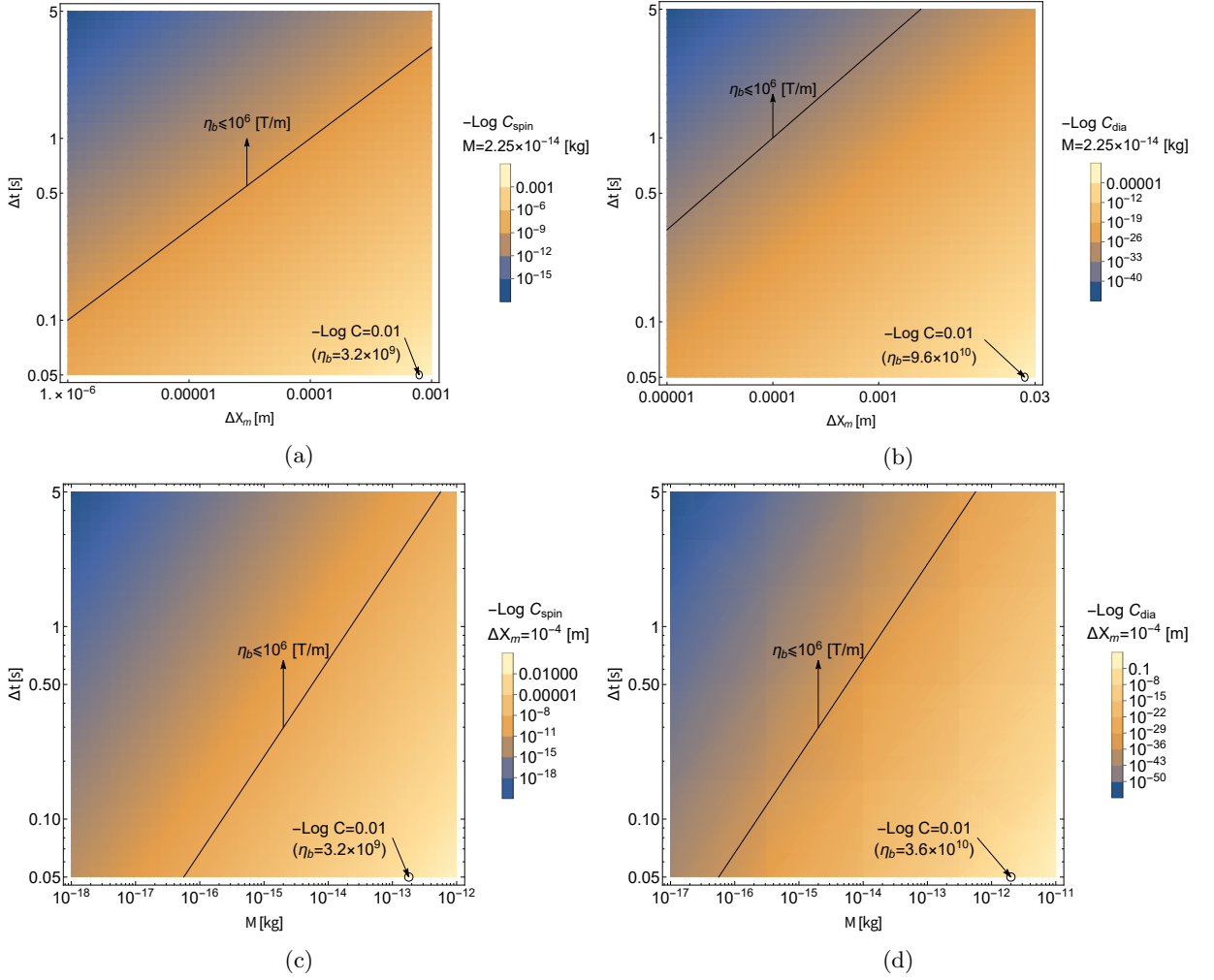
FIG. 6: Panels (a), (b), (c), and (d) illustrate the contrast reduction resulting from spin-magnetic field coupling and diamagnetic interaction under different scenarios, where the colour shading from dark to light represents progressively intensified contrast reduction. The first column corresponds to spin-magnetic field coupling, while the second corresponds to diamagnetic interaction. In the first row, (a) and (b) depict scenarios with a diamond mass of $M \sim 2.25 \times 10^{-14}$ kg, showing different maximum separations $\Delta X_{\rm m}$ (horizontal axis) and duration times Δt (vertical axis). In the second row, (c) and (d) assume a desired separation distance of $\Delta X_{\rm m} = 10^{-4}$m for the diamond's CoMs. We explore the contrast loss caused by phonon wavepackets of different masses under varying duration times. In the four subfigures depicted, we have marked the cases where the contrast loss reaches 1%. In subfigures (a) and (b), for a diamond with mass $M = 2.25 \times 10^{-14}$kg, significant contrast loss requires achieving maximum separation distances of approximately $\sim 10^{-3}$m and $\sim 10^{-2}$m for the centre-of-mass wave packet within 0.05s, respectively. In subfigures (c) and (d), to achieve $\Delta X_{\rm m} = 10^{-4}$m within 0.05 seconds, the diamond mass needs to reach approximately $\sim 10^{-13}$kg and 10^{-12}kg, respectively, to exhibit significant contrast loss. In these four cases marked, the magnetic gradients required are all large, becoming approximately 1000 to 10000 times greater than the current experimental capability.

imum separation distance $\Delta X_{\rm m}$ as time $t = 0$. Thus, $t_1 = -2\tau_{\rm a} - \tau_{\rm f}$, and $t_6 = -t_1 = 2\tau_{\rm a} + \tau_{\rm f}$.

To compute Eq. (25), we need to convert Eq. (10) and Eq. (11) into respective transfer functions. Here, we first provide their forms in the temporal domain as differences

on both sides of the interferometer arms,

$$
\begin{aligned}
\Delta F_s(t) &= \mu(S^{\rm R} - S^{\rm L})\eta_{\rm b} = 2\mu\eta_{\rm b} \\
\Delta F_{\rm dia}(t) &= N(F_c^R - F_c^L) \\
&= \frac{\chi_\rho M}{\mu_0}\eta_{\rm b}^2 \left(X_c^{\rm R} - X_c^{\rm L} \right).
\end{aligned}
\tag{27}
$$

The differential force for spin-phonon interaction is easily understood in (27). These are the constant differences between the left and right interferometer arms at differ-

ent time stages. Recall that η_b is the maximum value of the magnetic field gradient.

For the difference generated by diamagnetic repulsion, we have made an assumption: the diamagnetic repulsion experienced by the diamond as a bulk is averaged over each of its particles at its CoM, and we neglect the differences in diamagnetism between carbon atoms and nitrogen defects. Therefore, the summation over i in f_q of diamagnetic repulsion for each particle becomes the diamagnetic repulsion experienced by the central particle (averaged) multiplied by the number of particles N.

Thereafter, we can obtain their corresponding transfer functions,

$$
\begin{aligned}
|\Delta \tilde{f}_s(\omega_q)|^2 &= M \left(\frac{2\Delta X_m}{\tau_a^2 \omega_q}\right)^2 \times \Gamma^2(\omega_q) \\
|\Delta \tilde{f}_{dia}(\omega_q)|^2 &= M^5 \left(\frac{\chi_\rho \Delta X_m^3}{2\mu_0 \mu^2 \tau_a^6 \omega_q^3}\right)^2 \times \Gamma^2(\omega_q).
\end{aligned}
\tag{28}
$$

In Sec. 3, the coupling of the magnetic field with the spin generates the spatial superposition state of the diamond wave packet. Here, we parameterize the trajectory, acceleration, magnetic field gradient, and other parameters of the wave packet in terms of the acceleration duration τ_a, mass M, and maximum separation distance ΔX_m. The $\Gamma(\omega_q)$ here arises from the Fourier transform. For the two types of interactions, their forms are the same,

$$
\begin{aligned}
\Gamma(\omega_q) = \sin[(\tau_f)\omega_q] &- 2\sin[(\tau_a + \tau_f)\omega_q] \\
&+ \sin[(2\tau_a + \tau_f)\omega_q].
\end{aligned}
\tag{29}
$$

Substituting the corresponding transfer function in Eq.(28) into equation Eq.(25), we can obtain the expression for the contrast reduction brought about by these interactions,

$$
\begin{aligned}
-\text{Log}\, C_{spin} = \\
\sum_q \coth\left(\frac{1}{2}\frac{\hbar\omega_q}{k_B T}\right) \frac{M\Delta X_m^2}{\tau_a^4 \omega_q^3 \hbar}\Gamma^2(\omega_q),
\end{aligned}
\tag{30}
$$

$$
\begin{aligned}
-\text{Log}\, C_{dia} = \\
\sum_q \coth\left(\frac{1}{2}\frac{\hbar\omega_q}{k_B T}\right) \frac{\chi_\rho^2}{16\mu_0^2\mu^4\hbar}\frac{M^5\Delta X_m^6}{\tau_a^{12}\omega_q^7}\Gamma^2(\omega_q).
\end{aligned}
\tag{31}
$$

In Fig. 5, we show the contrast reduction resulting from spin-magnetic field and diamagnetic interactions in a setup with $\Delta t = 1$s. The horizontal axis represents the maximum separation distance of the diamond's centre of mass in the spatial superposition state. The black and red lines compare diamonds of different masses, solid and long dash lines represent results at low temperature (4 K), while dotted and short dash lines correspond to room temperature (300 K). The results indicate that the contrast loss induced by the spin-magnetic field coupling is dominant, while the effect of diamagnetic interaction is

significantly smaller. The source of these differences can be easily understood by comparisons in (30, 31). The contrast reduction caused by spin-magnetic field-phonon interaction is suppressed by ω_q^3, whereas the contrast loss caused by phonon-diamagnetic repulsion is suppressed by ω_q^7. [5]

Moreover, room temperature does not drastically alter the outcomes for either of them. Additionally, it can be observed that larger diamond masses lead to more phonon contrast reduction, which is quite understandable. Larger mass implies a lower range of phonon frequencies. From Eqs. (25) and (28), it can be seen that these ω_q terms appear in the denominators.

From Eq.(25), we can see that the acceleration protocol profoundly impacts the contrast of the phonon wave packets. In Fig. 6, we use a density plot to detail the contrast reduction resulting from different acceleration protocols. In the four subplots, we highlight the black curve, where the magnetic field gradient is precisely 10^6 T/m, and in the region above it, the duration time is longer, thus requiring a smaller magnetic field gradient. In Fig. 6(a) and (b), we study the contrast of a diamond with a mass of $M = 2.25 \times 10^{-14}$ kg under different maximum separation distances ΔX_m and duration times. In the QGEM, the separation distance of the CoM wave packets should be sufficiently large (e.g., $\Delta x \sim 10^{-4}$ m). We can observe that under a one-second flight time, the contrast loss resulting from spin-magnetic field coupling and diamagnetic interaction ranges from 10^{-9} to 10^{-6}

———————

[5] Since the main contribution of contrast loss comes from the fundamental frequency $\omega_0 \sim c/L$. One can consider two limits here, one is $\hbar\omega_0 \ll k_B T$ and the other is $\hbar\omega_0 \gg k_B T$. For the former limit, the square of the transfer function will yield the maximum value of $|\Gamma(\omega_0)|^2 \sim 1$, and Eqs. (30) and (31) become, respectively,

$$
-\text{Log}\, C_{spin} \approx \frac{2k_B T}{\hbar^2}\frac{M\Delta X_m^2}{\tau_a^4 \omega_0^4} \sim \frac{2k_B T}{\hbar^2}\rho\left(\frac{\Delta X_m}{c^2\tau_a^2}\right)^2 L^7,
$$

$$
-\text{Log}\, C_{dia} \approx \frac{k_B T\chi_\rho^2}{8\hbar^2\mu_0^2\mu^4}\frac{M^5\Delta X_m^6}{\tau_a^{12}\omega_0^8} \sim \frac{k_B T\chi_\rho^2\rho^5}{8\mu_0^2\mu^4\hbar^2}\left(\frac{\Delta X_m^3}{c^4\tau_a^6}\right)^2 L^{23}.
$$

In the other limit, when $\hbar\omega_0 \gg k_B T$ the hyperbolic function goes $\coth\frac{1}{2}\frac{\hbar\omega_0}{k_B T} \to 1$. The contrast reductions from the two interactions become as,

$$
-\text{Log}\, C_{spin} \approx \frac{M\Delta X_m^2}{\hbar\tau_a^4\omega_0^3} \sim \frac{\rho}{\hbar c^3}\left(\frac{\Delta X_m L^3}{\tau_a^2}\right)^2,
$$

$$
-\text{Log}\, C_{dia} \approx \frac{\chi_\rho^2}{16\mu_0^2\mu^4\hbar}\frac{M^5\Delta X_m^6}{\tau_a^{12}\omega_0^7} \sim \frac{\chi_\rho^2}{16\mu_0^2\mu^4\hbar}\frac{\rho^5}{c^7}\left(\frac{\Delta X_m^3 L^{11}}{\tau_a^6}\right)^2.
$$

In the above two limits, we have used the relation: $M = \rho L^3$, where ρ is the density of test masses and L is the length. In either of the limits, one can always conclude that more rigid material (which means faster sound speed) and smaller size of the test masses will produce less reduction in contrast. The diamond-like crystal will be an example of an ideal crystal for the QGEM experiment.

and 10^{-33} to 10^{-26}, respectively. In (c) and (d), we set the CoM's maximum separation distance to 10^{-4} m and explore the contrast loss for different diamond masses and duration times.

Consistent with intuition, larger masses lead to larger volumes, thus involving more phonon modes. A larger mass requires larger acceleration to create a large spatial superposition, hence a large force to be imparted on the diamond. The larger force leads to a significant loss, in contrast. For instance, at $\Delta t = 0.05$ s, a diamond with a mass of 10^{-12} kg will experience a contrast reduction of approximately 1% due to spin-magnetic field coupling. However, within the current experimental constraints where the SG magnetic field is constrained to be less than 10^6T/m [49, 72], the contrast loss induced by both couplings, e.g. spin and induced diamagnetic terms, is negligible for QGEM.

7. DISCUSSION

In this paper, we have analyzed the contrast loss due to phonon in creating spatial superposition of a nanoscaled diamond embedded with a single NV centre based on a Stern-Gaelach interferometer. During the process of creating a spatial superposition state using the coupling between the spin and the linear magnetic field, the spin particle in the lattice chain generates a pair of forces (10) of opposite directions and equal magnitudes due to their own spin superposition state. Similar to the Humpty-Dumpty problem at the centre of mass of the diamond, the spin particles on both sides of the interferometer arm have different vibrational states in the lattice, resulting in differences in the quantum states of the phonons. This also leads to imperfections in the overlap of phonon wave packets.

The other interaction arises from the diamagnetic properties of diamond. Each atom in the lattice chain produces a diamagnetic force (11) when subjected to an external magnetic field. This diamagnetic force is of the same direction but has a different magnitude on both sides of the interferometer arm. Similarly, due to this difference, the quantum states of phonons on both sides are also different, resulting in contrast reduction.

In this paper, we use a linear magnetic field (8), which is widely used in atomic interferometers. Furthermore, this linearity greatly simplifies the calculation of the motion state of spin particles. That is, the splitting force is independent of trajectories and the equilibrium position.

The situation is more complex regarding the interaction between diamagnetic force and phonons. Since the diamagnetic term in the Hamiltonian includes $B(X_i)^2$, the force on the lattice is now coupled with its trajectory. This external field mediated coupling between phonon and CoM's trajectory is common in the study of optical cooling of the motion state of diamond centre. In this work, we typically studied the latter situation and made comparison of contrast reduction between these two interactions.

Specifically, we assumed that the phonons were initially at a specific temperature T, and we utilized the Wigner representation to express and compute the evolution of the quantum state of the phonons.

Our results indicate that among these two sources contributing to the contrast loss in the phonon degrees of freedom, the effect of the spin-magnetic field coupling is dominant. The contrast loss induced by the diamagnetic term is smaller than the former, as shown in Fig. 5. This counter-intuitive result can be directly understood from (30) and (31). For the spin-magnetic field coupling, which does not depend on the trajectory, the contrast reduction is suppressed by the phonon frequency to the power of three. Meanwhile, the contrast loss due to diamagnetic interaction is suppressed by the phonon frequency to the power of seven.

The latter case directly arises from its coupling with the trajectory, as the diamagnetic force is a function of time, and its variation is adiabatic. In the seminal work [63, 64], this is also referred to as the degree of adiabaticity.

However, overall, the contrast reduction induced by both interactions is minimal. This is good news for matter-wave interferometers. There are two main reasons for this result. One is that we limit the gradient of the magnetic field. The most important reason, however, is that we are studying diamonds of very small size ($10^{-20} \sim 10^{-14}$ kg) compared to the speed of sound c multiplied by the duration time (on the order of microseconds and 1 second for QGEM). Since the frequencies of the phonons are very high (tens of gigahertz to several terahertz), their contribution to contrast loss is tiny. However, if we prefer a different material where the speed of sound is much smaller than that of the diamond, we would see the loss of contrast occur. However, it also depends on how we create the superposition; hence, it depends on the details of the transfer function.

[1] R. Penrose, Gen. Rel. Grav. **28**, 581 (1996).

[2] L. Diósi, Phys. Lett. A **129**, 419 (1988), arXiv:1812.11591 [quant-ph] .

[3] P. M. Pearle, Phys. Rev. A **39**, 2277 (1989).

[4] A. Bassi, K. Lochan, S. Satin, T. P. Singh, and H. Ul-bricht, Rev. Mod. Phys. **85**, 471 (2013), arXiv:1204.4325 [quant-ph] .

[5] S. Nimmrichter and K. Hornberger, Phys. Rev. Lett. **110**, 160403 (2013).

[6] C. Overstreet, P. Asenbaum, T. Kovachy, R. Notermans,

J. M. Hogan, and M. A. Kasevich, Phys. Rev. Lett. **120**, 183604 (2018).

[7] P. Asenbaum, C. Overstreet, M. Kim, J. Curti, and M. A. Kasevich, Phys. Rev. Lett. **125**, 191101 (2020).

[8] S. Bose, A. Mazumdar, M. Schut, and M. Toroš, Entropy **25**, 448 (2023), arXiv:2203.11628 [gr-qc] .

[9] S. Chakraborty, A. Mazumdar, and R. Pradhan, Phys. Rev. D **108**, L121505 (2023), arXiv:2310.06899 [gr-qc] .

[10] O. Romero-Isart, Phys. Rev. A **84**, 052121 (2011).

[11] O. Romero-Isart, A. C. Pflanzer, F. Blaser, R. Kaltenbaek, N. Kiesel, M. Aspelmeyer, and J. I. Cirac, Phys. Rev. Lett. **107**, 020405 (2011).

[12] O. Romero-Isart, M. L. Juan, R. Quidant, and J. I. Cirac, New J. Phys. **12**, 033015 (2010), arXiv:0909.1469 [quant-ph] .

[13] J. Tilly, R. J. Marshman, A. Mazumdar, and S. Bose, Phys. Rev. A **104**, 052416 (2021).

[14] M. Schut, J. Tilly, R. J. Marshman, S. Bose, and A. Mazumdar, Phys. Rev. A **105**, 032411 (2022).

[15] T. W. van de Kamp, R. J. Marshman, S. Bose, and A. Mazumdar, Phys. Rev. A **102**, 062807 (2020).

[16] S. Rijavec, M. Carlesso, A. Bassi, V. Vedral, and C. Marletto, New J. Phys. **23**, 043040 (2021), arXiv:2012.06230 [quant-ph] .

[17] F. Gunnink, A. Mazumdar, M. Schut, and M. Toroš, Class. Quant. Grav. **40**, 235006 (2023), arXiv:2210.16919 [quant-ph] .

[18] M. Schut, J. Tilly, R. J. Marshman, S. Bose, and A. Mazumdar, Phys. Rev. A **105**, 032411 (2022).

[19] M. Schut, H. Bosma, M. Wu, M. Toroš, S. Bose, and A. Mazumdar, (2023), arXiv:2312.05452 [quant-ph] .

[20] P. Fragolino, M. Schut, M. Toroš, S. Bose, and A. Mazumdar, (2023), arXiv:2307.07001 [quant-ph] .

[21] M. Toroš, A. Mazumdar, and S. Bose, (2020), arXiv:2008.08609 [gr-qc] .

[22] M. Schut, A. Grinin, A. Dana, S. Bose, A. Geraci, and A. Mazumdar, (2023), arXiv:2307.07536 [quant-ph] .

[23] R. J. Marshman, A. Mazumdar, G. W. Morley, P. F. Barker, S. Hoekstra, and S. Bose, New J. Phys. **22**, 083012 (2020), arXiv:1807.10830 [gr-qc] .

[24] E. Kilian, M. Toroš, F. F. Deppisch, R. Saakyan, and S. Bose, Phys. Rev. Res. **5**, 023012 (2023).

[25] P. F. Barker, S. Bose, R. J. Marshman, and A. Mazumdar, Phys. Rev. D **106**, L041901 (2022).

[26] A. Peters, K. Y. Chung, and S. Chu, Nature **400**, 849 (1999).

[27] R. Y. Chiao and A. D. Speliotopoulos, J. Mod. Opt. **51**, 861 (2004), arXiv:gr-qc/0312096 .

[28] A. Roura, D. R. Brill, B. L. Hu, C. W. Misner, and W. D. Phillips, Phys. Rev. D **73**, 084018 (2006).

[29] S. Foffa, A. Gasparini, M. Papucci, and R. Sturani, Phys. Rev. D **73**, 022001 (2006).

[30] S. Dimopoulos, P. W. Graham, J. M. Hogan, M. A. Kasevich, and S. Rajendran, Phys. Rev. D **78**, 122002 (2008).

[31] S. Dimopoulos, P. W. Graham, J. M. Hogan, M. A. Kasevich, and S. Rajendran, Physics Letters B **678**, 37 (2009).

[32] G. M. Tino et al., Eur. Phys. J. D **73**, 228 (2019), arXiv:1907.03867 [astro-ph.IM] .

[33] P. W. Graham, J. M. Hogan, M. A. Kasevich, and S. Rajendran, Phys. Rev. Lett. **110**, 171102 (2013).

[34] M.-Z. Wu, M. Toroš, S. Bose, and A. Mazumdar, Phys. Rev. D **107**, 104053 (2023), arXiv:2211.15695 [gr-qc] .

[35] S. Bose, A. Mazumdar, G. W. Morley, H. Ulbricht, M. Toroš, M. Paternostro, A. Geraci, P. Barker, M. S. Kim, and G. Milburn, Phys. Rev. Lett. **119**, 240401 (2017).

[36] S. Bose, https://www.youtube.com/watch?v=0Fv-0k13s_k (2016), accessed 1/11/22, on behalf of QGEM collaboration.

[37] C. Marletto and V. Vedral, Phys. Rev. Lett. **119**, 240402 (2017).

[38] D. Biswas, S. Bose, A. Mazumdar, and M. Toroš, Phys. Rev. D **108**, 064023 (2023), arXiv:2209.09273 [gr-qc] .

[39] F. Hanif, D. Das, J. Halliwell, D. Home, A. Mazumdar, H. Ulbricht, and S. Bose, (2023), arXiv:2307.08133 [gr-qc] .

[40] R. J. Marshman, A. Mazumdar, and S. Bose, Phys. Rev. A **101**, 052110 (2020).

[41] S. Bose, A. Mazumdar, M. Schut, and M. Toroš, Phys. Rev. D **105**, 106028 (2022).

[42] U. K. B. Vinckers, A. de la Cruz-Dombriz, and A. Mazumdar, Phys. Rev. D **107**, 124036 (2023), arXiv:2303.17640 [gr-qc] .

[43] S. G. Elahi and A. Mazumdar, Phys. Rev. D **108**, 035018 (2023), arXiv:2303.07371 [gr-qc] .

[44] M. Christodoulou et al., (2022), arXiv:2202.03368 .

[45] D. Carney, P. C. E. Stamp, and J. M. Taylor, Class. Quant. Grav. **36**, 034001 (2019).

[46] D. L. Danielson, G. Satishchandran, and R. M. Wald, Phys. Rev. D **105**, 086001 (2022).

[47] C. H. Bennett et al., Phys. Rev. A **54**, 3824 (1996).

[48] B. Friedrich and H. Schmidt-Böcking, (2021).

[49] S. Machluf, Y. Japha, and R. Folman, Nature communications **4**, 2424 (2013).

[50] Y. Margalit et al., (2020), 10.1126/sciadv.abg2879, arXiv:2011.10928 [quant-ph] .

[51] M. Schut, A. Geraci, S. Bose, and A. Mazumdar, (2023), arXiv:2307.15743 [quant-ph] .

[52] E. Joos, Physics and astronomy online library (Springer, 2003).

[53] M. Schlosshauer, Phys. Rept. **831**, 1 (2019), arXiv:1911.06282 [quant-ph] .

[54] R. J. Marshman, A. Mazumdar, R. Folman, and S. Bose, Phys. Rev. Res. **4**, 023087 (2022), arXiv:2105.01094 [quant-ph] .

[55] R. J. Marshman, S. Bose, A. Geraci, and A. Mazumdar, (2023), arXiv:2304.14638 [quant-ph] .

[56] M. Toroš, T. W. Van De Kamp, R. J. Marshman, M. S. Kim, A. Mazumdar, and S. Bose, Phys. Rev. Res. **3**, 023178 (2021).

[57] A. Großardt, Phys. Rev. A **102**, 040202 (2020).

[58] B. Englert, J. Schwinger, and M. O. Scully, Foundations of Physics **18**, 1045 (1988).

[59] J. Schwinger, M. O. Scully, and B. G. Englert, Zeitschrift für Physik D Atoms, Molecules and Clusters **10**, 135 (1988).

[60] M. O. Scully, B.-G. Englert, and J. Schwinger, Physical Review A **40**, 1775 (1989).

[61] B.-G. Englert, Zeitschrift für Naturforschung A **52**, 13 (1997).

[62] Y. Japha and R. Folman, (2022), arXiv:2202.10535 .

[63] C. Henkel and R. Folman, AVS Quantum Sci. **4**, 025602 (2022), arXiv:2112.01263 [quant-ph] .

[64] C. Henkel and R. Folman, (2023), arXiv:2305.15230 [quant-ph] .

[65] R. Zhou, R. J. Marshman, S. Bose, and A. Mazumdar, (2022), arXiv:2211.08435 .

[66] R. Zhou, R. J. Marshman, S. Bose, and A. Mazumdar, Phys. Rev. Res. **4**, 043157 (2022).

[67] R. Zhou, R. J. Marshman, S. Bose, and A. Mazumdar, Phys. Rev. A **107**, 032212 (2023), arXiv:2210.05689 [quant-ph] .

[68] Jishi, Radi A, (Cambridge University Press, 2013).

[69] W. B. Case, American Journal of Physics **76**, 937 (2008), https://pubs.aip.org/aapt/ajp/article-pdf/76/10/937/13118327/937_1_online.pdf .

[70] R. Zhou, R. J. Marshman, S. Bose, and A. Mazumdar, (2022), arXiv:2211.08435 [quant-ph] .

[71] C. Henkel, G. Jacob, F. Stopp, F. Schmidt-Kaler, M. Keil, Y. Japha, and R. Folman, New Journal of Physics **21**, 083022 (2019).

[72] H. J. Mamin, C. T. Rettner, M. H. Sherwood, L. Gao, and D. Rugar, Applied Physics Letters **100**, 013102 (2012).

Appendix A: Initial thermal equilibrium mixed state

Here, we provide supplementary information about characteristic length and characteristic velocity for phonons in (5). Consider that before any interaction between fields, the quantum oscillator system for mode q is,

$$H_{\text{free}} = \frac{1}{2}(\dot{u}_q^2 + \omega_q^2 u_q^2), \tag{A1}$$

the eigen-energy of this simple Hamiltonian is obvious $E_n = \hbar\omega_q(n + \frac{1}{2})$ where n is the phonon number in mode q. In this pure state, there is no ensemble to work with. Now, let us consider that initially, there are various phonon modes live in the diamond where they have reached a thermal equilibrium state with partition function,

$$
\begin{aligned}
Z &= \sum_n e^{-\beta E_n} \\
&= e^{-\frac{\beta}{2}\hbar\omega_q} \sum_{n=0}^{\infty} e^{-n\beta\hbar\omega_q} \\
&= \frac{1}{2\sinh\left(\frac{\beta}{2}\hbar\omega_q\right)}
\end{aligned}
\tag{A2}
$$

where $\beta = 1/k_{\text{B}}T$. The mathematical calculations from the second line to the third line in Eq. (A2) are somewhat complex, but this portion of the content can be found in any material related to thermodynamics and statistical mechanics. The average energy is, thus,

$$\langle E \rangle_q = -\frac{\partial \ln Z}{\partial \beta} = \frac{\hbar\omega_q}{2}\coth\left(\frac{\beta}{2}\hbar\omega_q\right) \tag{A3}$$

Note that the equipartition theorem tells us that the collection of phonon's potential energies and kinetic energies are the same, such that we have,

$$\left\langle \frac{\dot{u}_q^2}{2} \right\rangle = \left\langle \frac{\omega_q^2 u_q^2}{2} \right\rangle = \frac{\langle E \rangle_q}{2} = \frac{\hbar\omega}{4}\coth\frac{\hbar\omega}{2T}. \tag{A4}$$

Therefore, the square of characteristic width and velocity becomes,

$$\sigma_{\dot{u}_q}^2 = \langle \dot{u}_q^2 \rangle = \frac{\hbar\omega}{2}\coth\frac{\hbar\omega_q}{2k_{\text{B}}T}, \quad \sigma_{u_q}^2 = \langle u_q^2 \rangle = \sigma_{u_q}^2 = \frac{\hbar}{2\omega_q}\coth\frac{\hbar\omega_q}{2k_{\text{B}}T} \tag{A5}$$

Appendix B: Displacement and Wigner representation

Here, we supplement some details about Eq. (22). Based on the analysis from Fig. 3, we can consider the coupling between phonon modes after the natural frequency and magnetic field (spin-magnetic field-phonon interaction and phonon-diamagnetic force) as perturbations. Therefore, we can represent the time evolution of the phonon wavefunction in the interaction picture for a specific mode q as,

$$|\psi_{\text{I},q}^{\text{L,R}}(t)\rangle = \exp\left(-\frac{\text{i}}{\hbar}\int_0^t \text{d}t' V_q^{\text{L,R}}(t')\right)|\psi_q^{\text{L,R}}(0)\rangle \tag{B1}$$

We have set $|\psi_{\mathrm{I},q}(0)\rangle = |\psi_q(0)\rangle$ where $|\psi_q(0)\rangle$ is a stationary state in the Schrödinger picture. We have also ignored a global phase factor which does not contributes to the contrast. One can express the interaction potential in terms of phonon mode amplitude and momentum as,

$$
\begin{aligned}
V_q^{\mathrm{L,R}}(t) &= -\sum_i F_i^{\mathrm{L,R}} Q_q^i \sqrt{\frac{\hbar}{2M\omega_q}} (\hat{a}_{-q}^\dagger e^{i\omega_q t} + \hat{a}_q e^{-i\omega_q t}) \\
&= -\sum_i \left[\hat{u}_q \frac{F_i^{\mathrm{L,R}}}{\sqrt{M}} Q_q^i \cos(\omega_q t) + \hat{\dot{u}}_q \frac{F_i^{\mathrm{L,R}}}{\sqrt{M}} Q_q^i \frac{\sin(\omega_q t)}{\omega_q} \right] \\
&= -\hat{u}_q \cos(\omega_q t) f_q^{\mathrm{L,R}} - \hat{\dot{u}}_q \frac{\sin(\omega_q t)}{\omega_q} f_q^{\mathrm{L,R}}
\end{aligned}
\tag{B2}
$$

Where $f_q^{\mathrm{L,R}}$ has already been defined in Eq. (16) and the relation between creation, annihilation and phonon amplitude can be found in (2) and (3). The overlap of the wavefunctions of phonons on both sides of the interferometer arm can be expressed as:

$$
\begin{aligned}
&\langle \psi^{\mathrm{L}}(\Delta t)|\psi^{\mathrm{R}}(\Delta t)\rangle \\
&= \langle \psi_{\mathrm{I}}(0)| \exp\left\{ \frac{i}{\hbar} \int_0^{\Delta t} dt' \left[V_q^{\mathrm{L}}(t') - V_q^{\mathrm{R}}(t') \right] \right\} |\psi_{\mathrm{I}}(0)\rangle \\
&= \langle \psi_{\mathrm{I}}(0)| \exp\left\{ \frac{i}{\hbar} \int_0^{\Delta t} dt' \left[\hat{u}_q \cos(\omega_q t)\Delta f_q + \hat{\dot{u}}_q \frac{\sin(\omega_q t)}{\omega_q}\Delta f_q \right] \right\} |\psi_{\mathrm{I}}(0)\rangle
\end{aligned}
\tag{B3}
$$

The integral terms in the third line of Eq. (22) precisely represent the differences in phonon amplitudes and momentum given in Eq. (19). Here, one can observe that if the force acting on the atomic chain is coupled with spin and magnetic field, then $V_{\mathrm{I}}^{\mathrm{L}} = -V_{\mathrm{I}}^{\mathrm{R}}$. For diamagnetic interaction, since the diamagnetic force points in the same direction, the situation is different.

We use the Wigner representation to calculate the average of (22). under the Wigner representation, the average of an operator $\hat{A}(x)$ can be calculated as,

$$
\langle \hat{A} \rangle = \int \int W(x,p) \tilde{A}(x,p) \mathrm{d}x \mathrm{d}p
\tag{B4}
$$

where $W(x,p)$ is the Wigner function, it provides a quasi-distribution of quantum state simultaneously in position x and momentum p space. Usually, in the Wigner representation, one typically needs to utilize the Weyl transform to express the operator $\hat{A}$ as a function $\tilde{A}(x,p)$. In this context, the exponential operator in (B3) is already a function of phonon normal coordinates and their conjugates. We first consider a pure state of phonons in mode q, and its ground state wavefunction can be expressed as follows,

$$
\psi(u_q) = \left(\frac{\omega_q}{\pi\hbar} \right)^{1/4} e^{-\omega_q u_q^2/2\hbar}.
\tag{B5}
$$

The Wigner function is defined as,

$$
\begin{aligned}
W(u_q, \dot{u}_q) &= \frac{1}{2\pi\hbar} \int_{-\infty}^{\infty} e^{i\dot{u}_q y} \psi\left(u_q + \frac{y}{2} \right) \psi^*\left(u_q - \frac{y}{2} \right) \mathrm{d}y \\
&= \frac{1}{\pi\hbar} \exp\left[-\left(\frac{u_q^2}{2\left(\frac{\hbar}{2\omega_q}\right)} + \frac{\dot{u}_q^2}{2\left(\frac{\hbar\omega_q}{2}\right)} \right) \right]
\end{aligned}
\tag{B6}
$$

where $\frac{\hbar}{2\omega_q}$ and $\frac{\hbar\omega_q}{2}$ relate to characteristic width and velocity, respectively. In the thermal equilibrium mixed state, one needs to replace,

$$
\frac{\hbar\omega}{2} \to \frac{\hbar\omega}{2} \coth \frac{\hbar\omega_q}{2k_{\mathrm{B}}T}, \qquad \frac{\hbar}{2\omega_q} \to \frac{\hbar}{2\omega_q} \coth \frac{\hbar\omega_q}{k_{\mathrm{B}}T}.
\tag{B7}
$$

Appendix C: Contrast loss due to intrinsic dipole-phonon coupling

In this section, we present the contrast loss due to dipole-phonon coupling. It's worth noting that the dipole-phonon coupling we consider does not involve energy level transitions of the dipole, such as in the Jaynes-Cummings model. We only consider the overlap of the positions and momenta of the phonons on both sides of the interferometer arm, that is, the motion state of the phonons.

Here, let's first consider the case of an intrinsic dipole. In diamond materials embedded with NV centres, due to the NV centre itself carrying a negative charge, the inevitable occurrence of compensatory positive charges arises when it replaces a carbon atom in the material. As a result, a dipole moment d_0 arises, and its specific value depends on the distance from the compensatory positive charges to the NV centre. This value is approximately one Debye. Here, we aim to study the effect of the dipole on lattice vibrations through its interaction with an external electric field. Therefore, we assume that this intrinsic dipole overlaps with the NV centre, meaning that the compensatory positive charges and the NV centre are located in the same lattice site.

Same to the analysis in the main text, let us denote the position of a single intrinsic dipole as $X_c(t)+x_c$, where $X_c(t)$ represents the equilibrium position while x_c represent dipole's vibration. The dipole-phonon interaction Hamiltonian is again mediated by an extra electric field $E(X_c)$ as.

$$H_{\text{Intrinsic}} = -d_0 E(X_c) \tag{C1}$$

Recall that the diamond has its trajectories as illustrated in Fig. 2, the X_c can be expressed explicitly as (13) and $E(X_c)$ represents the electric field experienced by the dipole.

Again, due to the dipole being in a spatial superposition state (considering the diamond entering the SG apparatus), if there is a difference in the derivatives of $E(X_c)$ on both sides of the interferometer arm, there will be differences in the amplitudes and momentum of the phonons, as illustrated in (19). Obviously, if $E(X_c)$ is linear, the coupling between the dipole and the electric field will not cause such differences.

Appendix D: Contrast loss due to induced dipole-phonon coupling

This section presents an analysis of the induced dipole-phonon coupling on phonon contrast loss. Similarly, we only consider the motion state of the phonons and do not consider the energy level issues of the dipole. We consider that each particle i^{th} in the atomic chain experiences an external linear electric field,

$$E(X_i) = E_0 + \eta_e X_i(t) \tag{D1}$$

where the constant electric gradient is labeled as η_e. Again, particles move parallel to the diamond's trajectories, and their equilibrium positions X_i become functions of time. Due to the fact that the diamond is a dielectric material when subjected to the external electric field, an induced dipole will be generated in each atom of the lattice chain as,

$$d_i(X_i) = \frac{\alpha}{\epsilon_r} E(X_i) \tag{D2}$$

where $\epsilon_r \approx 5.7$ is the relative dielectric constant and the polarizability α is given by the Claussius-Mossotti relation,

$$\frac{\alpha N}{3\epsilon_0 V} = \frac{\epsilon_r - 1}{\epsilon_r + 2}. \tag{D3}$$

where V is the volume of the diamond. Therefore, the interaction Hamiltonian with the external electric field can be expressed as,

$$
\begin{aligned}
H_{\text{Induced}} &= -\sum_i d_i(X_i) E(X_i) \\
&= -\sum_i \frac{\alpha}{\epsilon_r} E^2(X_i)
\end{aligned}
\tag{D4}
$$

The force exerted on i^{th} particle can be written straightforwardly as,

$$F_i^{\text{dp}} = \frac{2\alpha}{\epsilon_r} E_0 \eta_e + \frac{2\alpha}{\epsilon_r} \eta_e^2 X_i \tag{D5}$$

The force acting on each polarized particle can be divided into two parts. The first term is the same on both sides of the interferometer arm, while the second term differs due to the spatial superposition state of the diamond. It should be noted that F_i here represents the force experienced by each polarized atom, and depending on their equilibrium positions, the force on each atom is different. However, since in this model, $X_{i+1} - X_i = $ const. where const. represents the distance between two atoms, therefore we have $X_i^L - X_i^R = \Delta X_c$. Substituting (D5) into (25) and (26), one can obtain the contrast loss caused by induced dipole-phonon interaction as,

$$C_{\mathrm{dp}} = \prod_q \exp\left[-\frac{\coth \frac{1}{2}\frac{\hbar\omega_q}{k_B T}}{\hbar\omega_q} \times \left|\frac{3V\Delta X_{\mathrm{m}}\eta_{\mathrm{e}}^2}{\tau_{\mathrm{a}}^2\omega_q^3}\frac{\epsilon_0(\epsilon_{\mathrm{r}}-1)}{\epsilon_{\mathrm{r}}(\epsilon_{\mathrm{r}}+2)} \times \Gamma(\omega_q)\right|^2\right] \tag{D6}$$

where, $\Gamma(\omega_q)$ is related to the Fourier transform given in (29). Here, one can estimate that the contrast loss induced by the induced dipole is very weak. Taking the diamond masses of interest (10^{-20} to 10^{-14} kg) as an example, their phonon frequency ranges from tens of gigahertz to several terahertz. In this case, the first term in (D6) is approximately on the magnitude of 10^{-24}. For the absolute value term, even if one chooses the maximum value of $\Gamma(\omega_q)$ and specifies a splitting protocol that achieves a maximum splitting of around 100μm within one second, the order of magnitude of this term only reaches about $10^{-130} \times \eta_{\mathrm{e}}^4$. Consider a case where a single charge is held at a distance of 500μm away from the diamond, in this case the electric gradient reaches only to 30V/m^2. Even if one assumes that the distance between the free charge held from the diamond reaches 100nm, the electric field gradient at this point is approximately $\sim 10^{10}$V/m^2, which is not sufficient to increase the contrast caused by dipole-electric field-phonon coupling becomes negligible.